Published OnlineFirst March 27, 2013; DOI: 10.1158/1535-7163.MCT-12-1082

Molecular Cancer Therapeutics

Discovery of a Novel Orally Active Small-Molecule gp130 Inhibitor for the Treatment of Ovarian Cancer

Shili Xu[1], Fedora Grande[1,2], Antonio Garofalo[2], and Nouri Neamati[1]

Abstract

Interleukin (IL)-6 and Stat3 play key roles in ovarian cancer progression. However, the role of glycoprotein 130 (gp130), the signal transducer of this signaling axis, is not well-established. Currently, there are no small-molecule inhibitors of gp130 under clinical development. In this study, we show that gp130 is an attractive drug target in ovarian cancer due to its role in promoting cancer progression via the activation of its downstream Stat3 signaling. We also present preclinical studies of SC144, the first-in-class orally active small-molecule gp130 inhibitor. SC144 shows greater potency in human ovarian cancer cell lines than in normal epithelial cells. SC144 binds gp130, induces gp130 phosphorylation (S782) and deglycosylation, abrogates Stat3 phosphorylation and nuclear translocation, and further inhibits the expression of downstream target genes. In addition, SC144 shows potent inhibition of gp130 ligand–triggered signaling. Oral administration of SC144 delays tumor growth in a mouse xenograft model of human ovarian cancer without significant toxicity to normal tissues. *Mol Cancer Ther; 12(6); 937–49. ©2013 AACR.*

Introduction

Ovarian cancer is the fourth-leading cause of death in women with gynecologic diseases in the United States. About 70% of the ovarian cancer cases are diagnosed at the late and distant stage and therefore are poorly treatable (1). Prolonged use of paclitaxel and carboplatin in the standard treatment often induces drug resistance, causes ovarian cancer relapse, and eventually the death of patients (2). In this context, there is an urgent need for breakthrough drugs with effective therapeutic impact on ovarian cancer.

Gp130 is part of the receptor signaling complexes for at least 8 cytokines [interleukin (IL)-6, IL-11, IL-27, LIF, CNTF, OSM, CT-1, and CLC; ref. (3)]. Ligand binding induces the association of gp130 with a cytokine-specific receptor-α chain, followed by the activation of downstream signaling cascades including JAK/STAT, RAS/RAF/MAPK, and PI3K/AKT pathways (4). It has been shown that phosphorylation of gp130 at Ser782 downregulates cell surface expression of gp130 (5, 6). As a ubiquitously expressed receptor, gp130 is involved in a wide range of important biologic processes including inflammation, autoimmunity, cancer (7), stem cell maintenance, and embryonic development (8). In recent years, increasing attention has been paid to the relationship between gp130 and cancer progression. However, the role of gp130 in ovarian cancer progression remains elusive, and there is a dearth of small-molecule inhibitors selectively targeting gp130.

Previously, we discovered novel quinoxalinhydrazides to have desirable physicochemical and drug-like properties and a broad-spectrum anticancer activity (9–11). Here, we show that the lead compound, SC144, is a first-in-class small-molecule gp130 inhibitor with oral activity in ovarian cancer.

Materials and Methods

Reagents

SC144, a quinoxalinhydrazide derivative, was synthesized as described (9). Stattic, a Stat3 inhibitor (12), was purchased from Sigma-Aldrich. Stock solutions of 10 mmol/L SC144 and Stattic were prepared in dimethyl sulfoxide (DMSO) and stored at −20°C. Further dilutions were made fresh in cell culture medium. IL-6, IFN-γ, and platelet-derived growth factor (PDGF) were purchased from PeproTech. LIF was purchased from Santa Cruz Biotechnology. SDF-1α plasmid was a generous gift from Dr. Ghalib A. Alkhatib (Indiana University, Indianapolis, IN) and the protein was expressed and purified as described (13). Anti-phospho-Stat3 (Y705, 9145), anti-Stat3 (9132), anti-gp130 (3732), anti-phospho-Stat1 (Y701, 9171), anti-Stat1 (9172), anti-Cyclin D1 (2978), anti-Bcl-X_L (2764), anti-Bcl2 (2870), anti-phospho-Akt (T308, 2965), anti-phospho-Akt (S473, 4060), anti-Akt (9272), and anti-Ape1 (4128) were purchased from Cell Signaling Technology.

Authors' Affiliations: [1]Department of Pharmacology and Pharmaceutical Sciences, School of Pharmacy, University of Southern California, Los Angeles, California; and [2]Dipartimento di Farmacia e Scienze della Salute e della Nutrizione, Università della Calabria, Arcavacata di Rende, Italy

Note: Supplementary data for this article are available at Molecular Cancer Therapeutics Online (http://mct.aacrjournals.org/).

Corresponding Author: Nouri Neamati, Department of Pharmacology and Pharmaceutical Sciences, School of Pharmacy, University of Southern California, Los Angeles, CA 90033. Phone: 323-442-2341; Fax: 323-442-1390; E-mail: neamati@usc.edu

doi: 10.1158/1535-7163.MCT-12-1082

Published OnlineFirst March 27, 2013; DOI: 10.1158/1535-7163.MCT-12-1082

Anti-phospho-gp130 (Ser782, 12978-R), anti-actin (1616-R), normal rabbit IgG (3888), and goat anti-rabbit IgG-HRP (2030) were purchased from Santa Cruz Biotechnology. Anti-gp130 (B-R3, 852-060-000) was purchased from Cell Sciences. Mouse IgG2a (010-0141) and goat anti-mouse IgG-HRP (610-1302) were purchased from Rockland. Goat anti-mouse Cy5-linked IgG and goat anti-rabbit Cy5-linked were purchased from GE Life Sciences. gp130 siRNA, Stat3 siRNA, control siRNA, siRNA transfection reagent, and siRNA transfection medium were purchased from Santa Cruz Biotechnology. Trypan Blue 0.4% solution was purchased from Lonza Inc.

Cell culture

OVCAR-8, OVCAR-5, and OVCAR-3 cells (National Cancer Institute, Developmental Therapeutics Program, Bethesda, MD) were maintained in RPMI-1640 supplemented with 10% heat-inactivated FBS (Gemini-Bioproducts). NCI/ADR-RES cells (National Cancer Institute) were maintained in RPMI-1640 supplemented with 10% heat-inactivated FBS and 5 mmol/L L-glutamine. HEY and Caov-3 cell lines were kindly provided as gifts by Dr. Louis Dubeau (University of Southern California, Keck School of Medicine, Los Angeles, CA). HEY cells were maintained in Dulbecco's Modified Eagle Media (DMEM) supplemented with 10% heat-inactivated FBS and 5 mmol/L L-glutamine. Caov-3 were maintained in MEM supplemented with 10% heat-inactivated FBS. Human normal kidney epithelial and human normal endometrial epithelial cells were kindly provided by Dr. Alan Epstein (University of Southern California, Keck School of Medicine) and maintained in RPMI-1640 supplemented with 10% heat-inactivated FBS. Cells were grown as monolayers at 37°C in a humidified atmosphere of 5% CO_2. To remove adherent cells from the flask for subculture and counting, cells were washed with PBS without calcium or magnesium, incubated with a small volume of 0.25% trypsin–EDTA solution (Mediatech, Inc.) for 5 to 10 minutes, resuspended with culture medium, and centrifuged. All experiments were carried out using cells in the exponential growth phase. Cells were routinely checked for *mycoplasma* contamination by using PlasmoTest (InvivoGen).

Colony formation assay

Colony formation assays were conducted as described (14). Briefly, OVCAR-8 cells (600 cells/well) and Caov-3 cells (800 cells/well) were seeded in 24-well plates and allowed to attach. After 48 hours, serial dilutions of the corresponding compounds or antibodies were added to the culture medium and incubated for 48 hours. Cells were cultured until colonies were formed (10 days for OVCAR-8 and 15 days for Caov-3), then subsequently washed, stained with crystal violet solution (2%) for 1 hour, and thoroughly washed with water.

Western blotting

Cells (only attached cells were collected) or xenograft tumor tissues were washed with ice-cold PBS and lysed in cold lysis buffer (20 mmol/L Tris-HCl, 150 mmol/L NaCl, 1 mmol/L EDTA, 1% Triton X-100, pH 7.5) with 1× protease and phosphatase inhibitors. Protein concentration was determined by BCA protein assay (Thermo Scientific). Proteins were resolved on 8% or 10% SDS-PAGE and electrotransferred to Immun-Blot PVDF membrane (Bio-Rad). After blocking with 5% milk in Tris-buffered Saline with Tween-80 (TBST), membranes were probed with the indicated primary antibodies, subsequently with horseradish peroxidase–conjugated secondary antibody, and developed using Dura Extended Duration Substrate (Thermo Scientific). Immunoreactive proteins were visualized with the Chemi-Doc System (Bio-Rad).

Growth inhibition assay

Growth inhibition was assessed using an MTT assay as described earlier (15). Cells were seeded in 96-well microtiter plates, allowed to attach 24 hours before siRNA transfections or the addition of corresponding compounds to the culture medium. After 72 hours, cells were incubated with 0.3 mg/mL MTT (Amresco) for an additional 3 hours at 37°C. After removal of the supernatant, DMSO was added to the wells and the absorbance was read at 570 nm. All assays were conducted in triplicate. Percentage of cell growth inhibition was expressed as: $(1 - A/C) \times 100\%$ (A and C were the absorbance values from experimental and control cells, respectively). Inhibitory concentration 50% (IC_{50}) values were determined for each drug from a plot of log (drug concentration) versus percentage of cell growth inhibition. SDs were calculated on the basis of the IC_{50} values obtained from at least 3 independent experiments.

DARTS assay

The Drug Affinity Responsive Target Stability (DARTS) assay was optimized and used to assess the binding of SC144 to gp130 via the protease protection from pronase (Roche Applied Science, Inc.) as previously described (16, 17). OVCAR-8 cells were lysed using M-PER (Thermo Scientific, Inc.) supplemented with protease and phosphatase inhibitors. The supernatant of cell lysate containing 4 to 6 μg/μL total proteins was incubated with SC144 at indicated concentrations at room temperature for 1 hour, followed by proteolysis with 1 μg pronase to every 9,600 μg of lysate for 30 minutes at room temperature. Final concentration of DMSO was 1% in all samples. To stop proteolysis, 5× SDS sample loading buffer [Tris-HCl 0.25 mol/L, pH 6.8, SDS 10%, glycerol 50%, bromophenol blue 0.5%, dithiothreitol (DTT) 100 mmol/L] was added to each sample at a 1:4 ratio, mixed well, and boiled at 100°C for 5 minutes. Samples were analyzed by Western blotting.

Published OnlineFirst March 27, 2013; DOI: 10.1158/1535-7163.MCT-12-1082

Annexin V–FITC apoptosis assay

OVCAR-8 and Caov-3 cells (2×10^5) were seeded in 35-mm dishes, allowed to attach overnight, and then received indicated treatments. Cells were washed with cold PBS. Both floating and attached cells were collected, stained with the Annexin V–FITC Apoptosis Detection Kit (BioVision) according to the manufacturer's protocol. The resulting fluorescence was measured by an LSR II flow cytometer (Becton Dickinson).

Fluorescence confocal microscopy

OVCAR-8 cells were grown on poly-L-lysine (Sigma-Aldrich)–coated glass coverslips and subjected to serum-free RPM1-1640 overnight. With or without compound pretreatments, cells were stimulated with 50 ng/mL IL-6 for 20 minutes (for Stat1) or 10 minutes (for Stat3), 50 ng/mL LIF for 15 minutes, or 50 ng/mL IFN-γ for 20 minutes. Cells were then fixed with 3.7% formaldehyde in PBS for 15 minutes at room temperature and permeabilized for 10 minutes with ice-cold 100% methanol at −20°C. After blocking with 5% goat serum, slides were incubated with anti-Stat1 (1:200) or anti-Stat3 (1:1,000) antibodies overnight at 4°C, followed by simultaneous incubation with Cy5-linked goat anti-mouse or goat anti-rabbit secondary antibody (1:1,000) and 100 nmol/L SYTOX Green nucleic acid stain (Invitrogen) at room temperature for 1 hour. Images were collected on a Leica TCS SP confocal system with ×40 or ×100 magnification.

siRNA transfections

siRNAs for gp130 (siGP130.1: Santa Cruz, #sc-29333; siGP130.2, siGP130.3, siGP130.4: OriGene, #SR302381) and Stat3 (siSTAT3.1: Santa Cruz, #sc-29493; siSTAT3.2: Santa Cruz, #sc44275) were used in this study. Subconfluent OVCAR-8 cells were transfected in 6- or 96-well plates with 80 nmol/L gp130, Stat3, or control siRNA according to the manufacturer's protocol. Protein expression was tested by immunoblotting after 72 hours of siRNA exposure. Cell viability was evaluated by MTT staining after 48, 72, and 96 hours of siRNA exposure.

Mice

Athymic mice (Charles River Laboratories) were used for *in vivo* efficacy studies. Mice were fed *ad libitum* and kept in air-conditioned rooms at 20°C ± 2°C with a 12-hour light–dark period. Animal care and manipulation were in agreement with the USC institutional guidelines, which were in accordance with the Guidelines for the Care and Use of Laboratory Animals.

In vivo tumor xenograft studies

OVCAR-8 cells in the logarithmic growth phase from *in vitro* cultures were implanted in athymic mice (5×10^5 cells in 100 μL of PBS/mouse) under aseptic conditions as previously described (18). Tumor growth was assessed by biweekly measurement of tumor diameters with a Vernier caliper. Tumor volume was calculated according to the formula: Tumor volume (mm^3) $= D \times d^2/2$, where D and d are the longest and shortest diameters, respectively. For intraperitoneal (i.p.) administration, tumors were allowed to grow to an average volume of 70 mm^3. Mice were then randomly assigned into 2 groups, 4 mice per group, for daily vehicle control or SC144 (10 mg/kg) treatment. To prepare SC144 solution for i.p. administration, 200 mg/mL DMSO stock solution of SC144 was diluted to 20 mg/mL in propylene glycol and further added to 0.9% NaCl with 40% propylene glycol. For oral administration, tumors were allowed to grow to an average volume of 40 mm^3. Mice were then randomly assigned into control (5 mice) and treatment (4 mice) groups. SC144 (100 mg/kg) was orally delivered every day to the treatment group. To prepare SC144 solution for oral administration, 300 mg/mL DMSO stock solution of SC144 was mixed with sesame oil. Mouse body weight and tumor volume were measured twice a week.

Histochemical analysis

Upon autopsy, tumors, kidneys, livers, pancreas, spleens, hearts, lungs, and brains from mice were collected, fixed in formalin, embedded in paraffin, and sectioned. Sections (4 μm) were stained with hematoxylin and eosin to facilitate histologic examination.

Immunohistochemistry

Immunohistochemistry was conducted on formalin-fixed, paraffin-embedded sections, following antigen retrieval. Internal hydrogen peroxidase activity was blocked with 3% hydrogen peroxide for 15 minutes. Tissue sections were subsequently blocked by Power block for 10 minutes and 10% goat serum for 30 minutes, followed by incubation with indicated antibodies at 4°C overnight. Anti-von Willebrand factor antibody (Dako, A0082) was kindly provided by Dr. Florence M Hofman (University of Southern California, Keck School of Medicine). Anti-Ki67 mAb (Thermo Scientific, RM-9106-S) was kindly provided by Dr. Bangyan Stiles (University of Southern California, School of Pharmacy). Anti-CD31 antibody (Santa Cruz Biotechnology, Inc., sc-8306) was kindly provided by Dr. Jason Wu. Anti-cleaved caspase-3 antibody was purchased from Cell Signaling, Inc. (9661). Tissue sections were then incubated with biotin-conjugated secondary antibody (BioGenex, HK337-5G) for 20 minutes and peroxidase-conjugated streptavidin (BioGenex, HK330-5K) for 20 minutes. TSA Plus Cyanine 3 Evaluation Kit (PerkinElmer, Inc., NEL744E001KT) was used to generate fluorescent signals, whereas nucleus was stained by 4′,6-diamidino-2-phenylindole (DAPI). Terminal deoxynucleotidyl transferase–mediated dUTP nick end labeling (TUNEL) staining was conducted according to manufacturer's instruction (Roche, 11 684 817 910).

Statistical analysis

The Student t test was used for statistical analysis and P value determination via SPSS 16.0 (SPSS Inc.) and Prism 5 (GraphPad Software, Inc.). Differences were considered statistically significant at $P < 0.05$.

Published OnlineFirst March 27, 2013; DOI: 10.1158/1535-7163.MCT-12-1082

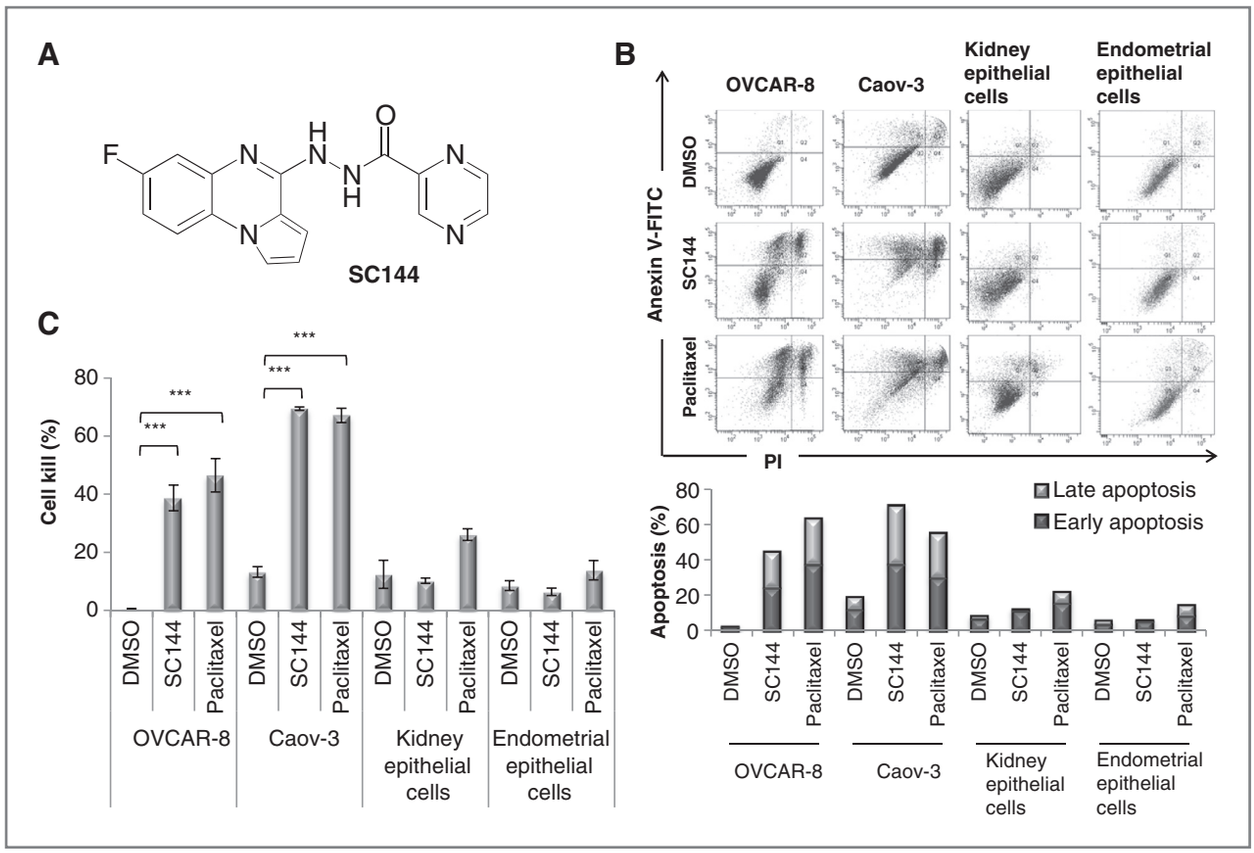

Figure 1. SC144 is cytotoxic to human ovarian cancer cell lines. A, chemical structure of SC144. B, SC144 causes significantly more apoptosis in OVCAR-8 and Caov-3 than normal kidney epithelial and normal endometrial cells. After treatment with SC144 (2 μmol/L), paclitaxel (2 μmol/L), or equal amount of DMSO for 72 hours, cells were stained with Annexin V–FITC and propidium iodide (PI) and then analyzed by flow cytometry. Top, cells in the bottom left quadrant of each panel (Annexin V–negative, PI-negative) are viable, whereas cells in the top left quadrant (Annexin V–positive, PI-negative) are in the early apoptotic stage, and cells in the top right quadrant (Annexin V–positive, PI-positive) are in the late apoptotic/necrotic stage. Bottom, the percentage of apoptotic cells is shown in a histogram. C, analysis of SC144 induced cell death in OVCAR-8, Caov-3, normal kidney epithelial, and normal endometrial cells. After treatment with SC144 (2 μmol/L), paclitaxel (2 μmol/L), or equal amount of DMSO for 72 hours, cells were stained with trypan blue. Histogram shows the percentage of trypan blue–stained cells after indicated treatment (***, $P < 0.001$; paired t test. Bar, SEM).

Results

SC144 shows cytotoxicity in a panel of human ovarian cancer cell lines

SC144 inhibits cell growth in a panel of human ovarian cancer cell lines with IC_{50} values in a submicromolar range (Table 1, Fig. 1A). The potency of SC144 toward NCI/ADR-RES (paclitaxel- and doxorubicin-resistant, IC_{50} = 0.43 μmol/L; refs. 19–21) and HEY (cisplatin-resistant, IC_{50} = 0.88 μmol/L) suggests an ability to overcome drug resistance in ovarian cancer. SC144 also inhibited colony formation in Caov-3 and OVCAR-8 cells (Supplementary Fig. S1A). We compared the abilities of SC144 to induce apoptosis and cell death in human ovarian cancer cells (OVCAR-8 and Caov-3) with human normal epithelial cells (kidney epithelial cells and endometrial epithelial cells). The kidney epithelial cells and the endometrial epithelial cells do not express cancer specific marker survivin (Supplementary Fig. S1B; ref. 22). SC144 induced

Table 1. Cytotoxicity of SC144 in a panel of human ovarian cancer cell lines

	IC_{50},[a] μmol/L						
	OVCAR-8	OVCAR-5	OVCAR-3	Caov-3	SKOV-3	HEY	NCI/ADR-RES
SC144	0.72 ± 0.32[b]	0.49 ± 0.44	0.95 ± 0.35	0.44 ± 0.14	0.53 ± 0.04	0.88 ± 0.46	0.43 ± 0.12

[a]IC_{50} is defined as the drug concentration causing a 50% decrease in the cell population.
[b]Values (mean ± SD) are calculated from 3 independent experiments.

Published OnlineFirst March 27, 2013; DOI: 10.1158/1535-7163.MCT-12-1082

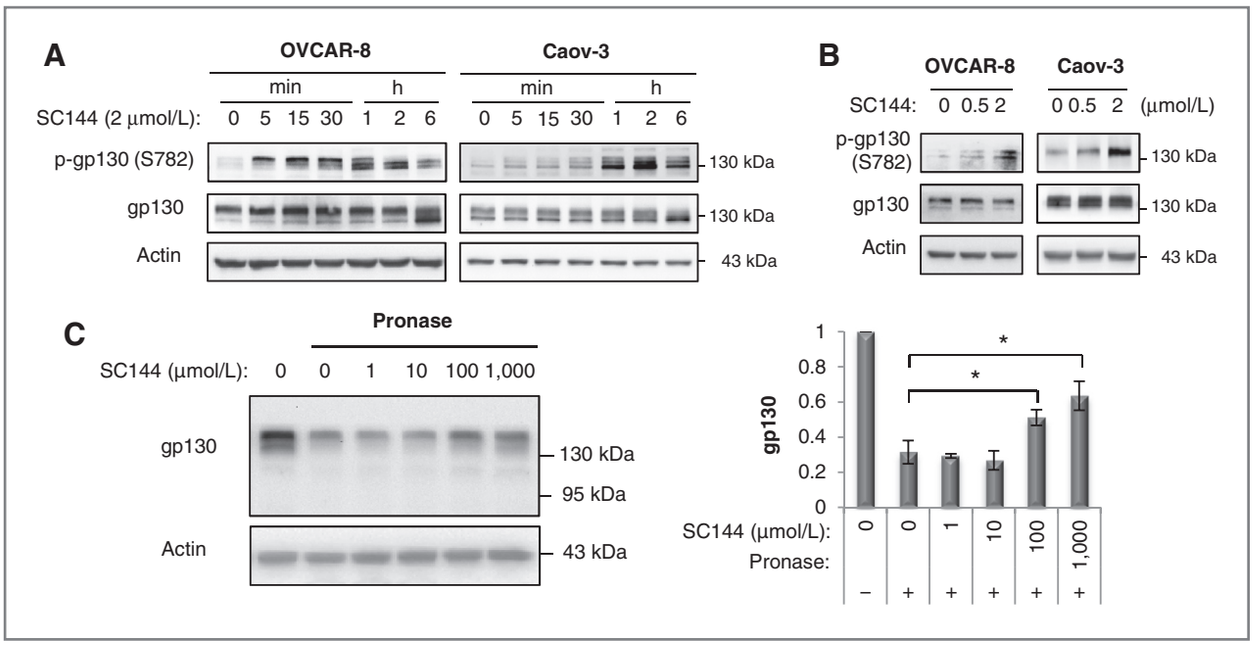

Figure 2. SC144 induces gp130 phosphorylation and deglycosylation. Immunoblot detection of phosphorylation of gp130 (Ser782) in OVCAR-8 and Caov-3 cells treated by SC144 in a time- (A) and dose-dependent (B) manner as indicated. C, SC144 directly binds gp130. OVCAR-8 cell lysate was used for the DARTS assay, conducted as described in Materials and Methods. Left, 1 of 3 representative experiments is shown. Right, statistical analyses of data from the 3 independent experiments. Error bars, SEM. *, $P < 0.05$; paired t test.

substantial apoptosis in OVCAR-8 and Caov-3 cells, but no considerable apoptotic effect was induced in the kidney epithelial cells or the endometrial epithelial cells (Fig. 1B). Consistently, trypan blue staining showed that SC144 significantly caused cell death in OVCAR-8 and Caov-3 cells, whereas no significant cell death was observed with SC144 treatment in the kidney epithelial cells or the endometrial epithelial cells (Fig. 1C). These results suggest that SC144 is preferentially cytotoxic to human ovarian cancer cells.

SC144 induces gp130 (Ser782) phosphorylation and downregulates gp130 glycosylation

SC144 treatment substantially increased the phosphorylation of gp130 (S782) in both OVCAR-8 and Caov-3 cells in a time- (Fig. 2A) and dose-dependent manner (Fig. 2B). In both cell lines, total gp130 protein was detected as 2 individual bands in immunoblotting (Fig. 2A). Silencing of gp130 using siRNAs decreased the abundance of both bands (Supplementary Fig. S2A), confirming that both bands are gp130. Treatment of OVCAR-8 and Caov-3 cells with brefeldin A (BFA), an inhibitor of protein glycosylation produced a time-dependent shift of gp130 into the lower band (Supplementary Fig. S2B), indicating that the upper band represents glycosylated gp130 and the lower band represents unglycosylated or minimal core glycosylated gp130. After 6-hour continuous SC144 treatment in OVCAR-8 and Caov-3 cells, the upper bands of total gp130 shifted to the lower band (Fig. 2A), indicating that SC144 treatment induced gp130 deglycosylation following the stimulation of gp130 phosphorylation. Also, SC144 is mechanistically different from BFA, which did not induce gp130 phosphorylation (Supplementary Fig. S2C). In addition, we found that gp130 ligands IL-6 and LIF substantially enhanced Stat3 (Y705) phosphorylation, whereas the phosphorylation of gp130 (Ser782) was only increased by LIF treatment (Supplementary Fig. S2D). These results suggest that phosphorylation at Ser782 is cytokine-specific and is not required for gp130 activation. Serine phosphorylation of surface receptors is often associated with receptor internalization. Therefore, we further examined the effect of SC144 treatment on cell surface gp130 abundance. SC144 significantly induced gp130 internalization at 10 μmol/L with 6- and 24-hour treatment, whereas at 0.5 and 2 μmol/L, no significant changes were detected at cell surface gp130 (Supplementary Fig. S2E).

Induction of gp130 phosphorylation and deglycosylation suggest that SC144 targets gp130. Binding of a small-molecule compound to its target protein can result in conformational changes and proteolytic stabilization of the protein by decreasing its sensitivity to proteases (17, 23). Similar in concept to DNA footprinting assay, DARTS assay (16, 17) was used to test the binding of SC144 to gp130. Incubation of SC144 with OVCAR-8 cell lysate protected gp130 from digestion in a dose-dependent manner as shown by the increased abundance of the gp130 band (Fig. 2C). Especially, 100 and 1,000 μmol/L of SC144 significantly increased gp130 abundance by 63% ($P = 0.035$) and 102% ($P = 0.020$) compared with vehicle control. These results show the direct binding of SC144 to gp130 and suggest that SC144

Published OnlineFirst March 27, 2013; DOI: 10.1158/1535-7163.MCT-12-1082

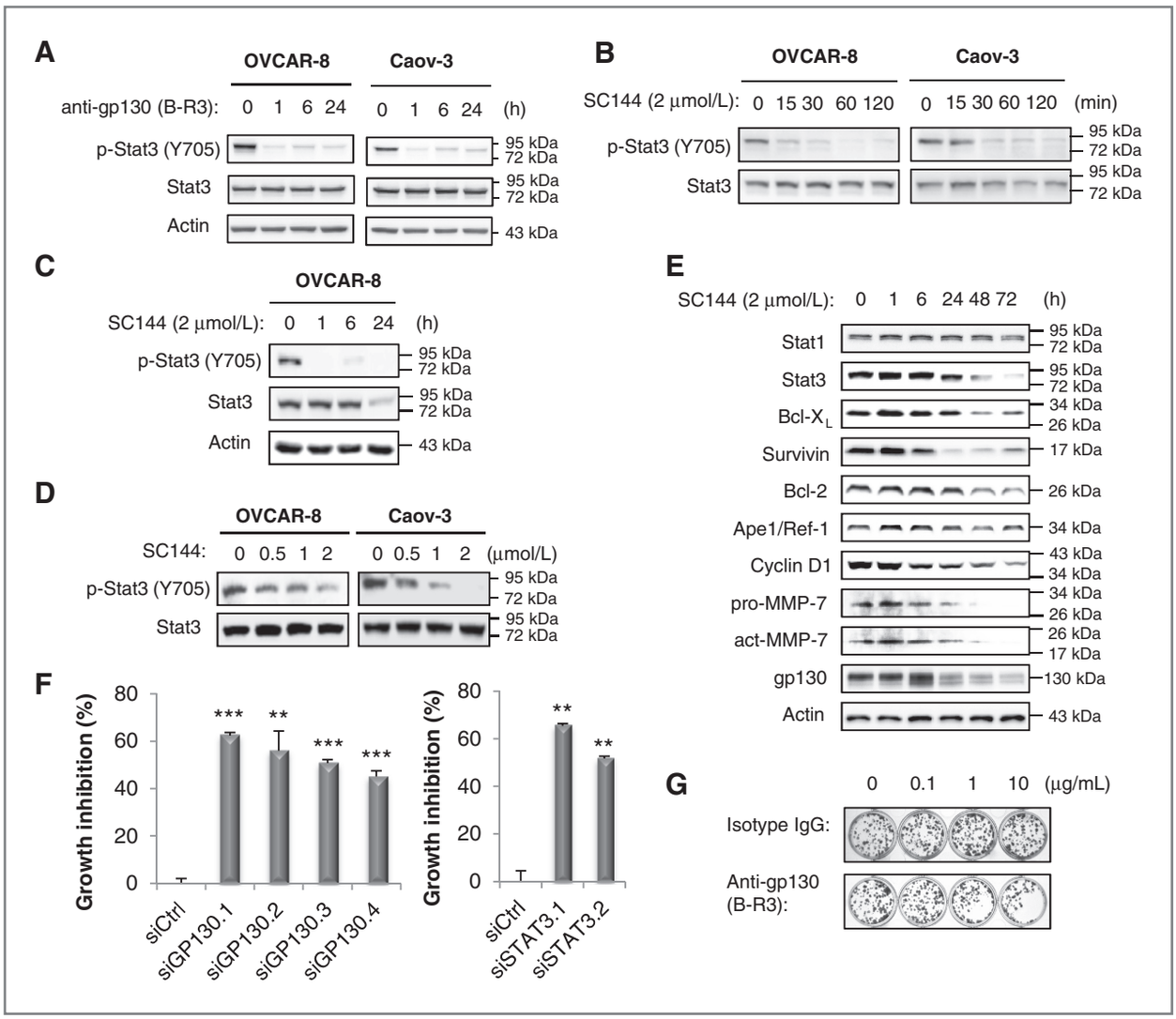

Figure 3. SC144 inhibits gp130/Stat3 signaling pathway. A, inhibition of Stat3 phosphorylation by anti-gp130 antibody. Protein extracts from OVCAR-8 and Caov-3 cells treated with a monoclonal antibody against an extracellular region (B-R3) of gp130 at 10 μg/mL for the indicated periods of time were analyzed for phospho-Stat3 (Ser782) and total Stat3. SC144 inhibited Stat3 (Y705) phosphorylation in OVCAR-8 and Caov-3 cells in a time-dependent manner at 2 μmol/L (B and C) and a dose-dependent manner after 1 hour (D). E, gp130/Stat3-mediated gene expression was inhibited in OVCAR-8 cells treated with SC144 (2 μmol/L) for the indicated periods of time. F, silencing of gp130 or Stat3 inhibited cell growth in ovarian cancer cells. An MTT assay was conducted 96 hours after the addition of indicated siRNAs. Bar, SEM. **, $P < 0.01$; ***, $P < 0.001$. G, colony formation in OVCAR-8 cells was inhibited by 48-hour treatment with anti-gp130 (B-R3) antibody at indicated concentrations.

may induce conformational changes in gp130 and affect its activity.

SC144 suppresses Stat3 signaling pathway

Treatment of OVCAR-8 and Caov-3 cells with an anti-gp130 (B-R3) antibody (Fig. 3A) or silencing of gp130 using siRNAs in OVCAR-8 cells (Supplementary Fig. S3A) substantially decreased constitutive Stat3 (Y705) phosphorylation. This suggests that the constitutive Stat3 activation is mainly maintained by extracellular gp130 ligands constitutively produced by ovarian cancer cells via an autocrine mechanism (24). Therefore, Stat3 activation could be used as a predictive marker for gp130 activity. SC144 treatment suppressed the constitutive phosphorylation of Stat3 (Y705) in a time- (Fig. 3B and C) and dose-dependent manner (Fig. 3D) in OVCAR-8 and Caov-3 cells. The total Stat3 level was decreased after 24 hours of SC144 treatment (Fig. 3C), perhaps due to an autoregulatory role of Stat3 (25). In comparison, Stattic, a previously reported Stat3 inhibitor (12), inhibited Stat3 (Y705) phosphorylation in OVCAR-8 cells in a time-dependent manner (Supplementary Fig. S3B). Moreover, Stattic exerted no substantial effect on phosphorylated and total gp130, indicating that SC144-induced gp130 phosphorylation and deglycosylation do not result from the direct inhibition of Stat3 (Y705) phosphorylation.

Published OnlineFirst March 27, 2013; DOI: 10.1158/1535-7163.MCT-12-1082

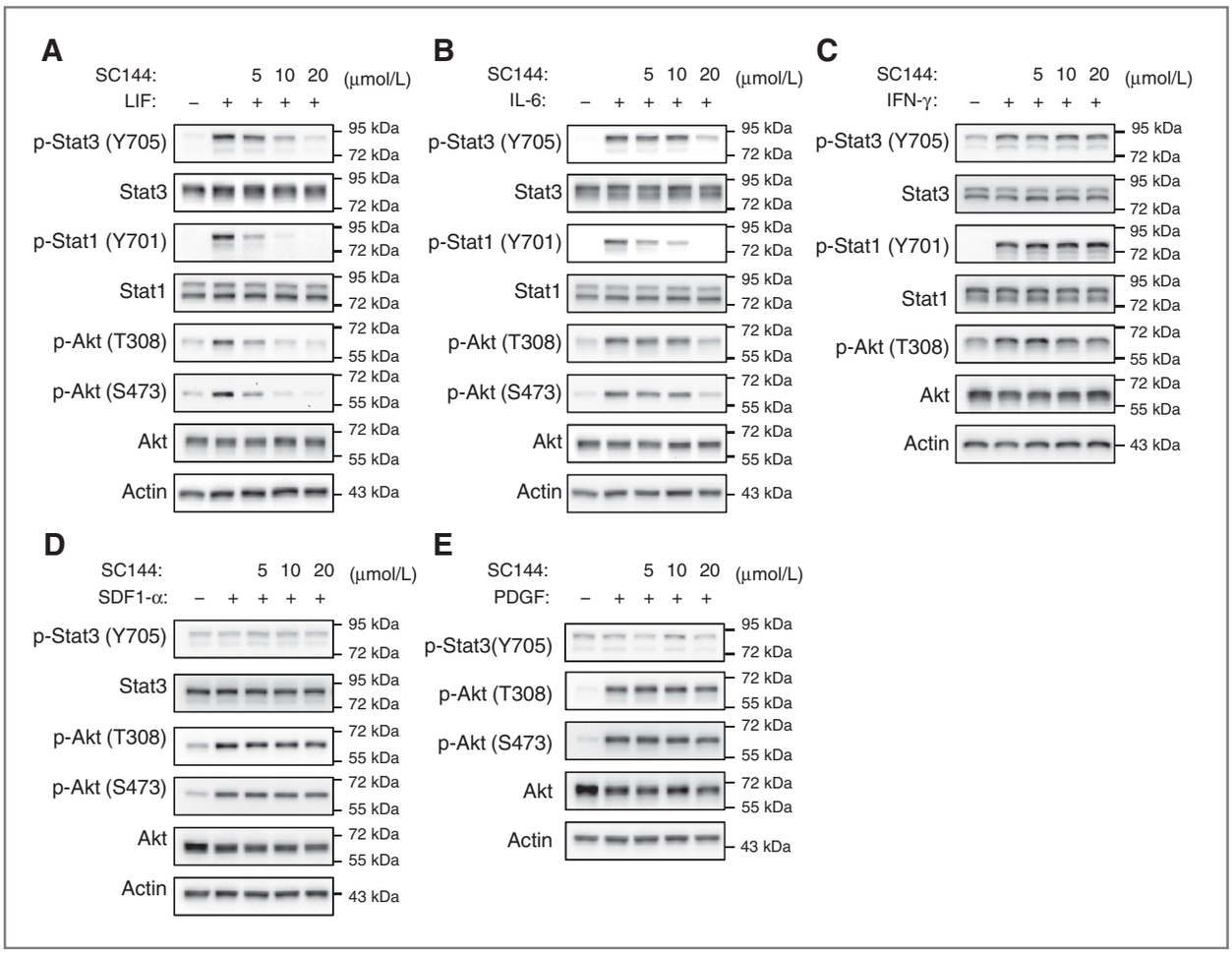

Figure 4. SC144 inhibits downstream signaling induced by gp130 cytokines. SC144 inhibits the downstream signaling elicited by LIF (A) or IL-6 (B) in a dose-dependent manner without affecting the downstream signaling induced by IFN-γ (C), SDF-1α (D), or PDGF (E). OVCAR-8 cells were serum-starved overnight before 4-hour pretreatment with SC144 at the indicated concentrations, followed by stimulation with LIF (50 ng/mL) for 15 minutes, IL-6 (50 ng/mL) for 10 minutes, IFN-γ (50 ng/mL) for 20 minutes, SDF-1α (80 ng/mL) for 10 minutes, or PDGF (20 ng/mL) for 15 minutes. Whole-cell lysates were subjected to immunoblotting using specific antibodies for the indicated proteins.

The activation of gp130/Stat3 promotes the expression of multiple genes (26), including Bcl-2 (27), Bcl-X_L (28), Cyclin D1 (29), survivin (29), Ape1/Ref-1 (30), and MMP-7 (31), which are involved in cell growth, survival, cell-cycle progression, proliferation, and metastasis. The role of gp130/Stat3 in promoting the expression of these genes in OVCAR-8 cells was confirmed by silencing of gp130 (Supplementary Fig. S4A) and Stat3 (Supplementary Fig. S4B). Importantly, silencing of Stat3 also reduced gp130 expression, which is consistent with a previous study unveiling a STAT-binding element located in the gp130 promoter region (29). To assess the effects of SC144 on the expression of gp130/Stat3-regulated genes, we treated OVCAR-8 cells with SC144 at various times. Survivin and MMP-7 were the most sensitive to SC144 treatment; their abundance was significantly decreased during the first 24 hours (Fig. 3E), whereas cyclin D1, Bcl-X_L, Bcl-2, and Ape1/Ref-1 expression started to decrease after 24 hours. Consistent with the Stat3 knockdown data, gp130 level was also significantly reduced within the first 24 hours of SC144 treatment. It is also important to point out that SC144 is mechanistically different from BFA due to the fact that total gp130 level was decreased after SC144 treatment but was increased after BFA treatment (Supplementary Fig. S2B). In addition, Stat1 was not affected by SC144 treatment. The inhibition of the gp130/Stat3 downstream effectors (Bcl-2, BclX_L, survivin, cyclin D1, Ape1/Rel-1, and MMP-7) further validates the mechanism of SC144 cytotoxicity in ovarian cancer cells. In addition, the cytotoxicity of SC144 (Supplementary Fig. S5A) as well as its inhibitory effects on gp130/Stat3 pathway (Supplementary Fig. S5B) were also observed in 2 pancreatic cancer cell lines, Panc-1 and Mia-Paca-2, suggesting its potential use for other cancers.

Published OnlineFirst March 27, 2013; DOI: 10.1158/1535-7163.MCT-12-1082

Taken together, these results confirm that SC144 inhibits the activation of the Stat3 signaling pathway downstream of gp130.

We further assessed whether the inhibition of gp130/Stat3 signaling contributes to the cytotoxicity of SC144 in ovarian cancer cells. By using gp130 siRNAs or Stat3 siRNAs, we found that silencing of gp130 or Stat3 significantly inhibited OVCAR-8 cell growth (Fig. 3F). While anti-gp130 (B-R3) antibody substantially reduced the ability of OVCAR-8 cells to form colonies in a dose-dependent manner (Fig. 3G), it only induced limited apoptosis (Supplementary Fig. S6A) compared with that triggered by SC144 (Fig. 1B), suggesting there may be additional mechanisms contributing to SC144-induced apoptosis. Furthermore, pharmacologic suppression of Stat3 activity by Stattic inhibited cell growth in OVCAR-8, Caov-3, and NCI/ADR-RES cells (Supplementary Fig. S6B). Taken together, these results show that the gp130/Stat3 inhibition results in cytotoxicity in human ovarian cancer cells.

SC144 potently blocks cytokine-triggered gp130 signaling

We compared the effects of SC144 on the activation of downstream signaling stimulated by gp130 cytokines, including LIF and IL-6, and non-gp130 cytokines, including an IFN family member IFN-γ, a GPCR (CXCR4) ligand SDF-1α, and a growth factor PDGF. SC144 inhibited LIF-induced phosphorylation of Stat3 (Y705) and Stat1 (Y701) in a dose- and time-dependent manner (Fig. 4A and Supplementary Fig. S7A). SC144 also inhibited LIF-induced Akt activation. Similar inhibitory effects of SC144 were observed on IL-6–stimulated phosphorylation of Stat3, Stat1 and Akt (Fig. 4B). We further examined the inhibitory effect of SC144 against different concentrations of IL-6. IL-6 stimulates Stat3 phosphorylation in a dose-dependent manner (Supplementary Fig. S7B). When 50 ng/mL IL-6 was used to induce Stat3 phosphorylation, SC144 exhibited the inhibitory effect at over 10 μmol/L (Supplementary Fig. S7C). When 3 ng/mL IL-6, which is close to the IL-6 concentration in the human body (24), was used to induce Stat3 phosphorylation, SC144 showed inhibitory effect at 2 μmol/L and a complete inhibition at 5 μmol/L. These results suggest that SC144 inhibits the downstream signaling activation elicited by gp130 ligands. In contrast, SC144 did not affect the activation of phosphorylation of Stat3, Stat1, and Akt stimulated by IFN-γ (Fig. 4C). Akt phosphorylation induced by SDF-1α (Fig. 4D) or PDGF (Fig. 4E) was not affected by SC144. Neither SDF-1α nor PDGF showed significant effects on Stat3 phosphorylation in OVCAR-8 (Fig. 4D and E). Our results show that the inhibitory effect of SC144 on the downstream signaling is gp130-specific and gp130-dependent.

The selectivity of SC144 in inhibiting the activation of downstream signaling stimulated by gp130 cytokines was also confirmed by examining the nuclear translocation of Stat3 and Stat1 induced by LIF, IL-6, or IFN-γ, which occurs following tyrosine phosphorylation. Immunofluorescence microscopy showed that SC144 treatment effectively inhibited LIF- and IL-6-induced nuclear translocation of Stat3 and Stat1 but was not able to affect STATs nuclear translocation induced by IFN-γ in OVCAR-8 cells (Fig. 5 and Supplementary Fig. S7D).

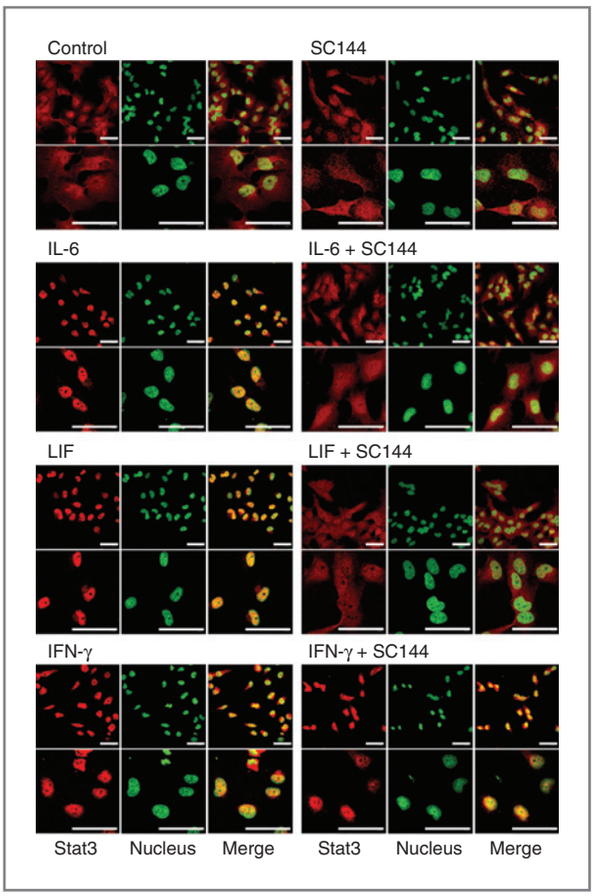

Figure 5. SC144 inhibits Stat3 nuclear translocation induced by gp130 cytokines. OVCAR-8 cells were serum-starved overnight before 4-hour pretreatment with or without SC144 (20 μmol/L), followed by stimulation with indicated cytokines. Images are representative of 3 independent experiments. Scale bar, 50 μm.

SC144 suppresses tumor growth in human ovarian cancer xenografts

To determine *in vivo* efficacy of SC144, we tested its effect on established tumors after subcutaneous inoculation of human ovarian cancer OVCAR-8 cells in the flank of nude mice. Compared with vehicle control treatment, daily i.p. administration of SC144 (10 mg/kg) for 58 days significantly inhibited tumor growth by about 73% (from $835.2 \pm 228.1\ mm^3$ to $228.1 \pm 92.5\ mm^3$; $P = 0.032$; Fig. 6A). To assess the oral bioavailability of SC144, we tested SC144 through daily oral administration. After we sacrificed the mice in the control group on day 69 due to their large tumors, we continued SC144 treatment for another 35 days. The average tumor volume in mice receiving daily oral administration of SC144 (100 mg/kg) was about

Published OnlineFirst March 27, 2013; DOI: 10.1158/1535-7163.MCT-12-1082

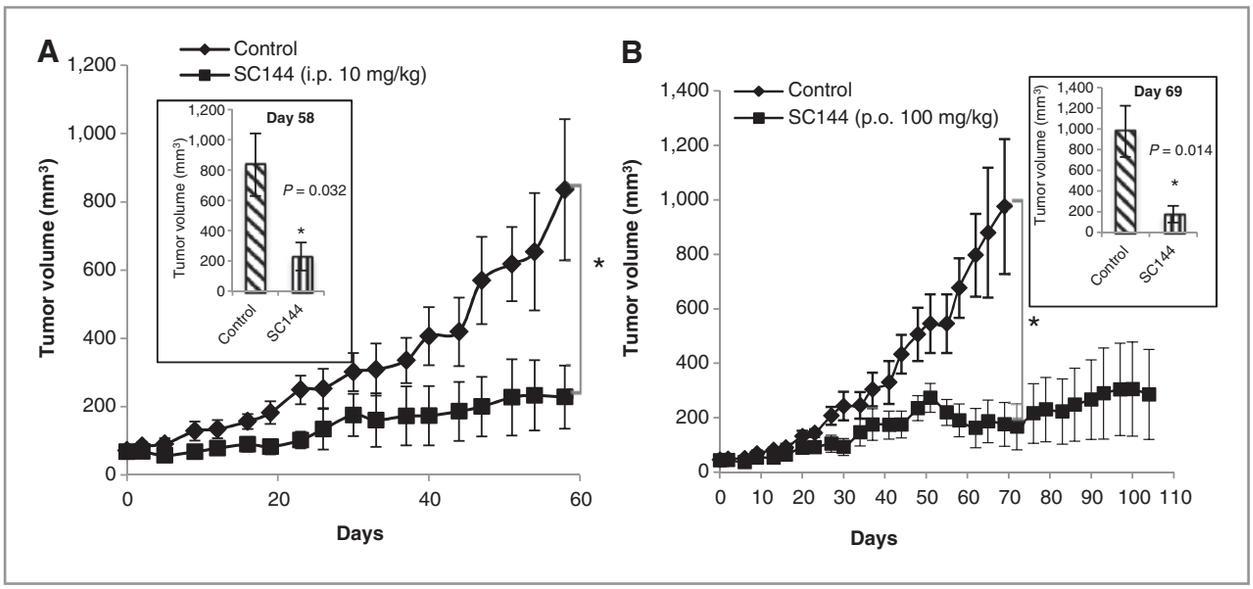

Figure 6. SC144 suppresses human ovarian cancer xenograft in nude mice. A, growth curves of s.c. tumors in nude mice treated with vehicle or SC144. OVCAR-8 tumor–bearing mice were treated daily with SC144 at 10 mg/kg ($n = 4$) or vehicle ($n = 4$) through i.p. injection for 5 days, followed by 2 days of rest over a treatment period of 58 days. B, growth curves of s.c. tumors in the SC144 [p.o. (oral)] treatment group ($n = 4$) or control group ($n = 5$). OVCAR-8 tumor–bearing mice were treated daily with or without SC144 (100 mg/kg) through oral administration for 5 days, followed by 2 days of rest. Mice in the control group were sacrificed on day 69. Mice in the treatment group were sacrificed after 104 days of SC144 treatment. Results are presented as mean ± SEM (*, $P < 0.05$).

82% smaller than that in the control group (on day 69, $975.8 \pm 247.9\,mm^3$ vs. $175.4 \pm 80.8\,mm^3$, $P = 0.014$; Fig. 6B). No significant body weight loss was detected during both treatment periods (Supplementary Fig. S8A and S8B). In addition, no substantial toxicity was observed in liver, kidney, spleen, lung, heart, pancreas, and brain (Supplementary Fig. S8C and S8D), further showing that SC144 did not produce significant adverse effects in mice at its effective anticancer dosage.

While the tumors excised from control mice appeared red, the ones from SC144-treated mice were pale (Fig. 7A), suggesting that SC144 treatment effectively inhibited tumor angiogenesis. SC144-induced reduction in tumor microvessel density was further confirmed by the significant decrease in both CD31 and von Willebrand factor (vWF) staining (Fig. 7A and Supplementary Fig. S8E). SC144 treatment also resulted in extensive areas of necrosis in the tumor (Fig. 7B and Supplementary Fig. S8F). Consistent with our in vitro data, SC144 treatment triggered apoptosis and suppressed cell proliferation in tumor, as is confirmed by the significant increase in TUNEL and cleaved caspase-3 staining and significant decrease in Ki67 staining, respectively (Fig. 7C and Supplementary Fig. S8G). The levels of gp130, MMP-7, Bcl-X_L, Bcl-2, and Ape1/Ref-1 in the tumor were substantially decreased in the SC144 treatment group (Fig. 7D), which is consistent with our *in vitro* data (Fig. 3E). Phospho-gp130 (S782) was decreased after SC144 treatment, which may result from the downregulation of total gp130 protein. The decrease in Bcl-X_L, Bcl-2, and Ape1/Ref-1 explains the extensive necrosis in the tumor tissue from the SC144 treatment mice due to the roles of these gp130 effectors in protecting cancer cells from apoptosis (32, 33), whereas the reduced level of MMP-7 contributes to both apoptosis and anti-angiogenesis (34, 35).

Discussion

IL-6 and Stat3 are involved in cancer progression and drug resistance in a variety of human cancers including ovarian cancer. Inhibition of IL-6 secretion by CDDO-Me induced apoptosis and sensitized drug-resistant ovarian cancer cells to paclitaxel and cisplatin (36). CNTO 328, a monoclonal antibody to IL-6, is currently in a phase I clinical trial for ovarian cancer. On the other hand, Stat3 is persistently active in ovarian cancer cell lines but not in normal ovarian epithelial cells (37). *In vitro* and *in vivo* studies confirmed that inhibition of constitutive Stat3 activation by using a Jak-selective inhibitor, a dominant-negative Stat3, or short hairpin RNA (shRNA) suppressed the growth and development of ovarian cancer (38–41). Considering that gp130 is positioned at the junction of this oncogenic signaling network and is decisive for the network activation, blocking gp130 activity using nonpeptidic small molecules is an attractive therapeutic approach to gp130-dependent cancers. However, so far no selective small-molecule gp130 inhibitors have been developed. In our study, we developed a quinoxalinhydrazide compound SC144 that inhibits gp130 cytokine signaling, as well as the downstream gene expression, and shows *in vitro* and *in vivo* potency in ovarian cancer. Because of the fact that the gp130 cytokine, IL-6, is

Published OnlineFirst March 27, 2013; DOI: 10.1158/1535-7163.MCT-12-1082

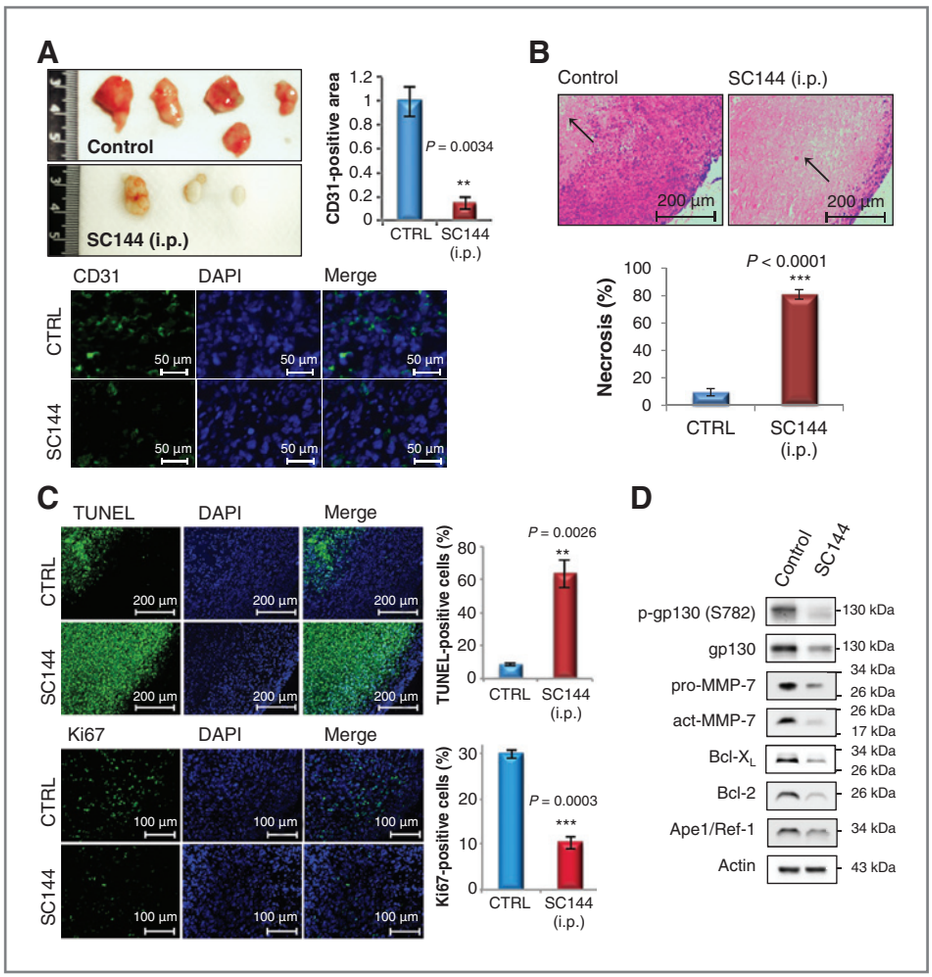

Figure 7. Effects of SC144 on *in vivo* ovarian tumor. A, SC144 treatment reduced tumor blood vessels in OVCAR-8 xenograft mice. Top left, tumors excised from i.p. vehicle-treated and SC144-treated mice are shown. Bottom, immunohistochemical staining for CD31. Percentage of positively stained areas was determined by the number of areas of stained microvessels divided by number of nuclei. Bar, SEM. **, $P < 0.01$. B, SC144 (i.p.) treatment induced extensive areas of necrosis in OVCAR-8 xenograft mice. Three different fields were used for quantification of areas of necrosis. Bar, SEM. ***, $P < 0.001$. C, immunohistochemical staining of TUNEL and Ki67. Percentage was determined by the number of double-stained cells divided by the number of nuclei. Bar, SEM. **, $P < 0.01$; ***, $P < 0.001$. D, SC144 (i.p.) treatment downregulated gp130/Stat3-mediated gene expression in OVCAR-8 tumors from xenograft mice.

constitutively produced and the key effectors (Stat3, Akt) in the gp130 downstream signaling pathways are persistently active in ovarian cancer (24, 42–44), ovarian cancer cells might be more sensitive to gp130 inhibitors than normal cells. This concept is in accord with our results that SC144 is more cytotoxic in human ovarian cancer cells than human normal epithelial cells and inhibits human ovarian tumor growth in a mouse xenograft model without obvious toxicity to normal tissues. To our knowledge, SC144 is the first-in-class small-molecule gp130 inhibitor with oral activity in ovarian cancer. In addition, our results showing that gp130 persistently activates Stat3 in ovarian cancer cells, promoting cell growth and proliferation, are consistent with a similar discovery in colitis-associated tumorigenesis (45). Although the identification of amino residues on gp130 that SC144 interacts and the elucidation of off-targets are beyond the scope of this present study, the following evidence cumulatively show that gp130 is directly inhibited by SC144: (i) SC144 binds to gp130 (Fig. 2C) and induces gp130 (S782) phosphorylation and deglycosylation (Fig. 2A and B); (ii) anti-gp130 antibody is able to completely suppress constitutive Stat3 activation (Fig. 3A), indicating that Stat3 activation as an indicator for the effect of SC144 on gp130; (iii) SC144 inhibits Stat3 activation and the expression of downstream genes (Fig. 3B–E); and (iv) SC144 potently inhibits the activation of the downstream signaling pathways stimulated by gp130 ligands but shows no effect on the activation of the downstream signaling pathways stimulated by non-gp130 ligands (Figs. 4 and Fig. 5 and Supplementary Fig. S7).

The role of phospho-S782 in gp130 was first documented in 2000 to downregulate gp130 cell surface expression (5). Recently, it has been reported that phospho-S782-associated downregulation of gp130 cell surface expression is mediated by immediate internalization (46). Indeed, phosphorylation of many transmembrane receptors at Ser/Thr residues is commonly associated with the negative modulation of receptor activity (47). The induction of gp130 deglycosylation and the decrease in total gp130 protein level may also contribute to Stat3 inhibition at a later time. However, it required 10 μM of SC144 to induce gp130 internalization (Supplementary Fig. S2E), a concentration higher than for triggering gp130 deglycosylation. This may suggest that the amount of deglycosylation induced by SC144 at 2 μmol/L may not be enough to

Published OnlineFirst March 27, 2013; DOI: 10.1158/1535-7163.MCT-12-1082

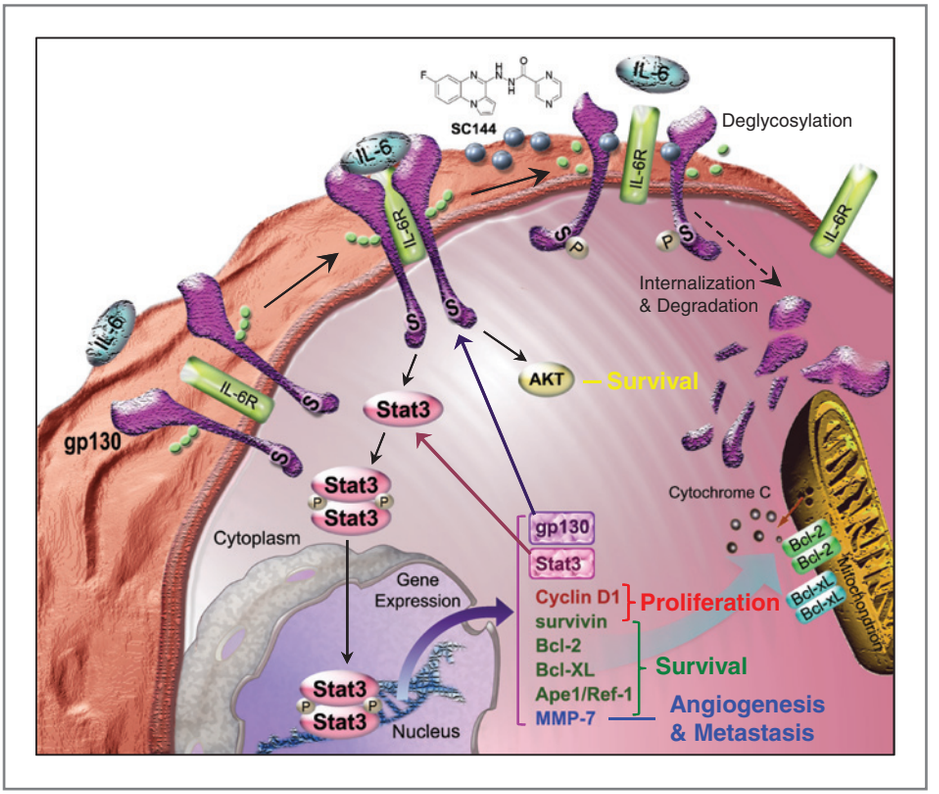

Figure 8. A working model for the anticancer mechanism of SC144 in ovarian cancer. We surmise that SC144 is cytotoxic to ovarian cancer cells via a mechanism involving the inhibition of gp130 activity, leading to the inactivation of Akt and Stat3 as well as the suppression of Stat3-regulated gene expression. As a result, SC144 treatment eventually causes cell-cycle arrest, anti-angiogenesis, and apoptosis.

immediately initiate receptor internalization. However, the *in vivo* concentration of SC144 exceeds 10 μmol/L under our experimental conditions. Moreover, inhibition of gp130/Stat3 amplifies the cytotoxicity of SC144 by downregulating the expression of several downstream genes, such as Bcl-2, Bcl-X_L, cyclin D1, MMP-7, Ape1/Ref-1, and survivin, in ovarian cancer cells that results in the submicromolar IC_{50} values after 72-hour SC144 treatment (Table 1).

On the basis of results presented in this study, we propose a plausible model for the anticancer mechanism of SC144 in ovarian cancer (Fig. 8). SC144 binding induces conformational changes and activity loss in the cell surface–bound gp130 receptor, exposing the Ser782 residue to protein kinases such as CaMKII, CaMKIV, and MK2 (6, 46). The decrease in gp130 activity leads to the inactivation of downstream signaling pathways involving Stat3 and Akt. The suppression of gp130/Stat3-mediated gene expression amplifies the potency of SC144 due to the inhibition of cell-cycle progression and angiogenesis and the promotion of apoptosis and cell death. In addition, the downregulation of the PI3K/Akt pathway also contributes to apoptosis and cell death. Our working model may serve to identify a unifying anticancer mechanism likely to be shared by future gp130 inhibitors.

Clinically, in patients with advanced ovarian cancer, high plasma levels of IL-6 correlate with poor prognosis (48, 49), and increased levels of IL-6 are also present in malignant ascites (50). Therefore, biopsy detection of IL-6 levels appears to be one strategy to identify subjects/patients who may benefit most from IL-6/gp130-blocking therapies. In addition, other components of the gp130 receptor complexes (e.g., OSMR-β, LIFR-β) as well as other gp130 cytokines (e.g., OSM) have been reported to be highly expressed in human ovarian carcinoma tissues and have the ability to activate downstream signaling pathways (e.g., Stat3 pathway; ref. 51). On the basis of such observations, these molecules can also be used as markers for selecting target subjects/patients. In fact, this evidence also supports that gp130 antagonists may be more effective for ovarian cancer treatment compared to IL-6 inhibitors (e.g., anti-IL-6 mAb), as other gp130 cytokines may compensate the effects of IL-6.

Disclosure of Potential Conflicts of Interest

No potential conflicts of interest were disclosed.

Authors' Contributions

Conception and design: S. Xu, N. Neamati
Development of methodology: S. Xu, F. Grande, A. Garofalo, N. Neamati
Analysis and interpretation of data (e.g., statistical analysis, biostatistics, computational analysis): S. Xu, F. Grande, A. Garofalo, N. Neamati
Writing, review, and/or revision of the manuscript: S. Xu, N. Neamati
Administrative, technical, or material support (i.e., reporting or organizing data, constructing databases): N. Neamati
Study supervision: N. Neamati

Acknowledgments

The authors thank Drs. Roger Duncan, Ebrahim Zandi, and Joe Miller for their comments and suggestions and also thank Dr. Bangyan Stiles for her kind assistance for immunohistochemical staining.

Grant Support

This study was supported by funds through the Department of Defense Ovarian Cancer Program (OCRP) Idea Award (W81XWH-07-1-0414) to N. Neamati.

The costs of publication of this article were defrayed in part by the payment of page charges. This article must therefore be hereby marked *advertisement* in accordance with 18 U.S.C. Section 1734 solely to indicate this fact.

Received November 12, 2012; revised February 25, 2013; accepted March 20, 2013; published OnlineFirst March 27, 2013.

References

1. Siegel R, Naishadham D, Jemal A. Cancer statistics, 2012. CA Cancer J Clin 2012;62:10–29.
2. Petty R, Evans A, Duncan I, Kurbacher C, Cree I. Drug resistance in ovarian cancer - the role of p53. Pathol Oncol Res 1998;4:97–102.
3. Jones SA, Scheller J, Rose-John S. Therapeutic strategies for the clinical blockade of IL-6/gp130 signaling. J Clin Invest 2011;121:3375–83.
4. Wang X, Lupardus P, Laporte SL, Garcia KC. Structural biology of shared cytokine receptors. Annu Rev Immunol 2009;27:29–60.
5. Gibson RM, Schiemann WP, Prichard LB, Reno JM, Ericsson LH, Nathanson NM. Phosphorylation of human gp130 at Ser-782 adjacent to the Di-leucine internalization motif. Effects on expression and signaling. J Biol Chem 2000;275:22574–82.
6. Gibson RM, Laszlo GS, Nathanson NM. Calmodulin-dependent protein kinases phosphorylate gp130 at the serine-based dileucine internalization motif. Biochim Biophys Acta 2005;1714:56–62.
7. Silver JS, Hunter CA. gp130 at the nexus of inflammation, autoimmunity, and cancer. J Leukoc Biol 2010;88:1145–56.
8. Rose-John S. GP130 stimulation and the maintenance of stem cells. Trends Biotechnol 2002;20:417–9.
9. Grande F, Aiello F, Grazia OD, Brizzi A, Garofalo A, Neamati N. Synthesis and antitumor activities of a series of novel quinoxalinhydrazides. Bioorg Med Chem 2007;15:288–94.
10. Plasencia C, Grande F, Oshima T, Cao X, Yamada R, Sanchez T, et al. Discovery of a novel quinoxalinhydrazide with a broad-spectrum anticancer activity. Cancer Biol Ther 2009;8:458–65.
11. Oshima T, Cao X, Grande F, Yamada R, Garofalo A, Louie S, et al. Combination effects of SC144 and cytotoxic anticancer agents. Anticancer Drugs 2009;20:312–20.
12. Schust J, Sperl B, Hollis A, Mayer TU, Berg T. Stattic: a small-molecule inhibitor of STAT3 activation and dimerization. Chem Biol 2006;13:1235–42.
13. Altenburg JD, Broxmeyer HE, Jin Q, Cooper S, Basu S, Alkhatib G. A naturally occurring splice variant of CXCL12/stromal cell-derived factor 1 is a potent human immunodeficiency virus type 1 inhibitor with weak chemotaxis and cell survival activities. J Virol 2007;81:8140–8.
14. Munshi A, Hobbs M, Meyn RE. Clonogenic cell survival assay. Methods Mol Med 2005;110:21–8.
15. Yamada R, Kostova MB, Anchoori RK, Xu S, Neamati N, Khan SR. Biological evaluation of paclitaxel-peptide conjugates as a model for MMP2-targeted drug delivery. Cancer Biol Ther 2010;9:192–203.
16. Lomenick B, Jung G, Wohlschlegel JA, Huang J. Target identification using drug affinity responsive target stability (DARTS). Curr Protoc Chem Biol 2011;3:163–80.
17. Lomenick B, Hao R, Jonai N, Chin RM, Aghajan M, Warburton S, et al. Target identification using drug affinity responsive target stability (DARTS). Proc Natl Acad Sci U S A 2009;106:21984–9.
18. Xu S, Butkevich AN, Yamada R, Zhou Y, Debnath B, Duncan R, et al. Discovery of an orally active small-molecule irreversible inhibitor of protein disulfide isomerase for ovarian cancer treatment. Proc Natl Acad Sci U S A 2012;109:16348–53.
19. Roschke AV, Tonon G, Gehlhaus KS, McTyre N, Bussey KJ, Lababidi S, et al. Karyotypic complexity of the NCI-60 drug-screening panel. Cancer Res 2003;63:8634–47.
20. Alvarez M, Paull K, Monks A, Hose C, Lee JS, Weinstein J, et al. Generation of a drug resistance profile by quantitation of mdr-1/P-glycoprotein in the cell lines of the National Cancer Institute Anticancer Drug Screen. J Clin Invest 1995;95:2205–14.
21. Lee JS, Paull K, Alvarez M, Hose C, Monks A, Grever M, et al. Rhodamine efflux patterns predict P-glycoprotein substrates in the National Cancer Institute drug screen. Mol Pharmacol 1994;46:627–38.
22. Altieri DC. Validating survivin as a cancer therapeutic target. Nat Rev Cancer 2003;3:46–54.
23. Park C, Marqusee S. Pulse proteolysis: a simple method for quantitative determination of protein stability and ligand binding. Nat Methods 2005;2:207–12.
24. Watson JM, Sensintaffar JL, Berek JS, Martinez-Maza O. Constitutive production of interleukin 6 by ovarian cancer cell lines and by primary ovarian tumor cultures. Cancer Res 1990;50:6959–65.
25. Ichiba M, Nakajima K, Yamanaka Y, Kiuchi N, Hirano T. Autoregulation of the Stat3 gene through cooperation with a cAMP-responsive element-binding protein. J Biol Chem 1998;273:6132–8.
26. Debnath B, Xu S, Neamati N. Small molecule inhibitors of signal transducer and activator of transcription 3 (Stat3) protein. J Med Chem 2012;55:6645–68.
27. Selvendiran K, Bratasz A, Tong L, Ignarro LJ, Kuppusamy P. NCX-4016, a nitro-derivative of aspirin, inhibits EGFR and STAT3 signaling and modulates Bcl-2 proteins in cisplatin-resistant human ovarian cancer cells and xenografts. Cell Cycle 2008;7:81–8.
28. Duan Z, Bradner JE, Greenberg E, Levine R, Foster R, Mahoney J, et al. SD-1029 inhibits signal transducer and activator of transcription 3 nuclear translocation. Clin Cancer Res 2006;12:6844–52.
29. Cai L, Zhang G, Tong X, You Q, An Y, Wang Y, et al. Growth inhibition of human ovarian cancer cells by blocking STAT3 activation with small interfering RNA. Eur J Obstet Gynecol Reprod Biol 2010;148:73–80.
30. Haga S, Terui K, Zhang HQ, Enosawa S, Ogawa W, Inoue H, et al. Stat3 protects against Fas-induced liver injury by redox-dependent and -independent mechanisms. J Clin Invest 2003;112:989–98.
31. Fukuda A, Wang SC, Morris JPt, Folias AE, Liou A, Kim GE, et al. Stat3 and MMP7 contribute to pancreatic ductal adenocarcinoma initiation and progression. Cancer Cell 2011;19:441–55.
32. Patel MP, Masood A, Patel PS, Chanan-Khan AA. Targeting the Bcl-2. Curr Opin Oncol 2009;21:516–23.
33. Fishel ML, Kelley MR. The DNA base excision repair protein Ape1/Ref-1 as a therapeutic and chemopreventive target. Mol Aspects Med 2007;28:375–95.
34. Ii M, Yamamoto H, Adachi Y, Maruyama Y, Shinomura Y. Role of matrix metalloproteinase-7 (matrilysin) in human cancer invasion, apoptosis, growth, and angiogenesis. Exp Biol Med (Maywood) 2006;231:20–7.
35. Sang QX. Complex role of matrix metalloproteinases in angiogenesis. Cell Res 1998;8:171–7.
36. Duan Z, Ames RY, Ryan M, Hornicek FJ, Mankin H, Seiden MV. CDDO-Me, a synthetic triterpenoid, inhibits expression of IL-6 and Stat3 phosphorylation in multi-drug resistant ovarian cancer cells. Cancer Chemother Pharmacol 2009;63:681–9.
37. Huang M, Page C, Reynolds RK, Lin J. Constitutive activation of stat 3 oncogene product in human ovarian carcinoma cells. Gynecol Oncol 2000;79:67–73.
38. Huang F, Tong X, Fu L, Zhang R. Knockdown of STAT3 by shRNA inhibits the growth of CAOV3 ovarian cancer cell line *in vitro* and *in vivo*. Acta Biochim Biophys Sin (Shanghai) 2008;40:519–25.
39. Burke WM, Jin X, Lin HJ, Huang M, Liu R, Reynolds RK, et al. Inhibition of constitutively active Stat3 suppresses growth of human ovarian and breast cancer cells. Oncogene 2001;20:7925–34.
40. Niu G, Heller R, Catlett-Falcone R, Coppola D, Jaroszeski M, Dalton W, et al. Gene therapy with dominant-negative Stat3 suppresses growth

Published OnlineFirst March 27, 2013; DOI: 10.1158/1535-7163.MCT-12-1082

of the murine melanoma B16 tumor *in vivo*. Cancer Res 1999;59: 5059–63.

41. Catlett-Falcone R, Landowski TH, Oshiro MM, Turkson J, Levitzki A, Savino R, et al. Constitutive activation of Stat3 signaling confers resistance to apoptosis in human U266 myeloma cells. Immunity 1999;10:105–15.
42. Nicosia SV, Bai W, Cheng JQ, Coppola D, Kruk PA. Oncogenic pathways implicated in ovarian epithelial cancer. Hematol Oncol Clin North Am 2003;17:927–43.
43. Liu X, Shi Y, Han EK, Chen Z, Rosenberg SH, Giranda VL, et al. Downregulation of Akt1 inhibits anchorage-independent cell growth and induces apoptosis in cancer cells. Neoplasia 2001;3:278–86.
44. Cheng JQ, Jiang X, Fraser M, Li M, Dan HC, Sun M, et al. Role of X-linked inhibitor of apoptosis protein in chemoresistance in ovarian cancer: possible involvement of the phosphoinositide-3 kinase/Akt pathway. Drug Resist Updat 2002;5:131–46.
45. Bollrath J, Phesse TJ, von Burstin VA, Putoczki T, Bennecke M, Bateman T, et al. gp130-mediated Stat3 activation in enterocytes regulates cell survival and cell-cycle progression during colitis-associated tumorigenesis. Cancer Cell 2009;15:91–102.
46. Radtke S, Wuller S, Yang XP, Lippok BE, Mutze B, Mais C, et al. Cross-regulation of cytokine signalling: pro-inflammatory cytokines restrict IL-6 signalling through receptor internalisation and degradation. J Cell Sci 2010;123:947–59.
47. Sibley DR, Benovic JL, Caron MG, Lefkowitz RJ. Regulation of transmembrane signaling by receptor phosphorylation. Cell 1987;48: 913–22.
48. Lutgendorf SK, Weinrib AZ, Penedo F, Russell D, DeGeest K, Costanzo ES, et al. Interleukin-6, cortisol, and depressive symptoms in ovarian cancer patients. J Clin Oncol 2008;26:4820–7.
49. Scambia G, Testa U, Benedetti Panici P, Foti E, Martucci R, Gadducci A, et al. Prognostic significance of interleukin 6 serum levels in patients with ovarian cancer. Br J Cancer 1995;71:354–6.
50. Plante M, Rubin SC, Wong GY, Federici MG, Finstad CL, Gastl GA. Interleukin-6 level in serum and ascites as a prognostic factor in patients with epithelial ovarian cancer. Cancer 1994;73:1882–8.
51. Savarese TM, Campbell CL, McQuain C, Mitchell K, Guardiani R, Quesenberry PJ, et al. Coexpression of oncostatin M and its receptors and evidence for STAT3 activation in human ovarian carcinomas. Cytokine 2002;17:324–34.

Published OnlineFirst March 27, 2013; DOI: 10.1158/1535-7163.MCT-12-1082

Molecular Cancer Therapeutics

Discovery of a Novel Orally Active Small-Molecule gp130 Inhibitor for the Treatment of Ovarian Cancer

Shili Xu, Fedora Grande, Antonio Garofalo, et al.

Mol Cancer Ther 2013;12:937-949. Published OnlineFirst March 27, 2013.